

Article

# Sustainability from the Occurrence of Critical Dynamic Power System Blackout Determined by Using the Stochastic Event Tree Technique

Muhammad Murtadha Othman \*, Nur Ashida Salim and Ismail Musirin

Faculty of Electrical Engineering, Universiti Teknologi MARA, 40450 Shah Alam, Selangor, Malaysia; nurashida606@salam.uitm.edu.my (N.A.S.); ismailbm@salam.uitm.edu.my (I.M.)

\* Correspondence: m\_murtadha@salam.uitm.edu.my; Tel.: +606-016-395-2703

Academic Editor: Tomonobu Senjyu

Received: 26 March 2017; Accepted: 31 May 2017; Published: 3 June 2017

**Abstract:** With the advent of advanced technology in smart grid, the implementation of renewable energy in a stressed and complicated power system operation, aggravated by a competitive electricity market and critical system contingencies, this will inflict higher probabilities of the occurrence of a severe dynamic power system blackout. This paper presents the proposed stochastic event tree technique used to assess the sustainability against the occurrence of dynamic power system blackout emanating from implication of critical system contingencies such as the rapid increase in total loading condition and sensitive initial transmission line tripping. An extensive analysis of dynamic power system blackout has been carried out in a case study of the following power systems: IEEE RTS-79 and IEEE RTS-96. The findings have shown that the total loading conditions and sensitive transmission lines need to be given full attention by the utility to prevent the occurrence of dynamic power system blackout.

**Keywords:** stochastic event tree technique; critical dynamic power system blackout; sensitive transmission line; total loading severity

---

## 1. Introduction

Congestion management is a challenging task for an Independent System Operator (ISO) that has the responsibility to ensure effectiveness and safety in the operation of a deregulated power system. This is because the system is increasingly stressed because of adverse impact from a competitive electricity market augmented by the uncertain operation of smart grid and renewable energy. Consequently, several implications of sensitive transmission line tripping and severe total loading condition include occurrence of severe blackouts being likely to be experienced by a deregulated power system operation. Therefore, it is imperative to seek a solution providing an early detection of sensitive transmission line and severe total loading condition in such a way that preventive action can be realized to prevent the emergence of power system blackout. The dynamic response of a system plays an imperative role in the analysis of power system security, especially when it entails a power system blackout, which is usually caused by the impact of enormous and unforeseen faults, unexpected generation and load outages, and abrupt increment of loads [1].

Several studies on the static power system blackout analysis have been deliberated in recent literature. The probability distribution function (PDF) of system blackout for the Oak Ridge-PSERC-Alaska (OPA) power system model was examined and investigated based on the adjustment of loading condition [2–5]. This method uses the DC power flow solution and the linear programming method to reduce the cost function of power system blackout. The obtained PDF of OPA power system blackout is then used to perform a risk assessment of system blackout for a different power system model.

However, the disadvantage of using the OPA power system model is that only a small number of nodes are required to construct a network model [6]. This is because the proposed method may cause exponential divergence of PDF for other types of large power system and result in inaccurate risk assessment for power system blackout. Another approach adopted to study the power system blackout phenomena is the CASCADE technique [4,5,7]. CASCADE technique is used to assess a general qualitative behavior that may be present in power system cascading failures. The acquired outcome will be risk assessment of a power system blackout that is purported to be relatively analogous to a small interruption. From the literature survey, it is noteworthy that the dynamic power system blackout has not been explored particularly for the determination of sensitive transmission lines and severe total loading conditions.

This paper will discuss the determination of sensitive transmission lines and severe total loading conditions as a result of a dynamic power system blackout caused by an initial tripping of transmission line. The dynamic power system blackout can be regarded as the propagation of system component tripping agitated by either an overloaded transmission line or violation of a synchronous generator rotor angle and frequency limits. Efficacy of the proposed stochastic event tree technique utilized in the risk assessment of a dynamic power system blackout is confirmed via the case study of the following power systems: IEEE RTS-RTS79 and IEEE RTS-96. It is imperative for the proposed stochastic event tree technique to consider the critical clearing time (CCT) of a protection relay, generator rotor angle, forced outage rate (FOR) of a generator, and simultaneous tripping of exposed transmission lines and generators in such a way that it is the basic approach that critically needs to be considered in the risk assessment of dynamic power system blackout. The abovementioned approach has not been considered and discussed in previous literature even though the stochastic event tree method has been used in the analysis of dynamic power system blackout [8–10]. As a compendium for this section, dynamic power system blackout should be assessed regularly by the utility in such a way that it will be useful to improvise an early stage of preventive action by identifying the sensitive transmission lines and severe total loading conditions.

## 2. Research Methodology

This section will discuss the One Machine Infinite Bus (OMIB) required to simplify a large scale of dynamic equivalent multi-machine system model. The OMIB equivalent model of a multi-machine system is implemented directly to determine the critical clearing time (CCT),  $t_{c_{OMIB}}$ , required in the risk assessment of a dynamic power system blackout for the determination of sensitive transmission lines and severity of loading conditions. A detail explanation and derivation of OMIB can be obtained by referring to the discussion in [11–13].

### 2.1. One Machine Infinite Bus (OMIB) Rotor Angle during Pre-Fault Condition

The main concept of one machine infinite bus (OMIB) model refers to a single machine equivalent (SIME) method that is carried out to simplify the computationally challenging factor of a multi-machine system with non-linear time domain simulation [14–16]. The following procedure will elaborate on the determination of rotor angle associated with the OMIB.

1. Distinguish between the critical,  $cm$ , and non-critical,  $ncm$ , machines identified with regards to the threshold, as explicated in Equation (1). The determination of critical and non-critical machines (Equation (1)) has been introduced in [17]. In particular, Li et al. [17] elucidated that the angular deviation of each generator with respect to the center of inertia (COI) can be used to overcome the difficulties in identifying the critical and non-critical machines. The same concept has also been implemented and discussed in [18–20]. In Equation (1), the  $\Delta\delta_n(t) > 0^\circ$  signifies that an

accelerating power occurred in the critical machines. On the other hand, the  $\Delta\delta_n(t) \leq 0^\circ$  implies that a decelerating power incurred in the non-critical machines.

$$ncm \cup cm = \begin{cases} cm & , \text{ if } \Delta\delta_n(t) \leq 0^\circ \\ m & , \text{ if } \Delta\delta_n(t) > 0^\circ \end{cases} \quad (1)$$

where

$$\Delta\delta_n(t) = \delta_n(t) - \delta_{COI}(t) \quad (2)$$

$$\delta_{COI}(t) \triangleq \frac{\left(\sum_{n=1}^G H_n \delta_n(t)\right)}{\left(\sum_{n=1}^G H_n\right)} \quad (3)$$

where  $H$  is the inertia driven by a synchronous machine (per unit); and  $G$  is the total number of generating units.

- Use Equations (8)–(10) and (14) to calculate the  $P_{m_{OMIB}}$ ,  $P_{c_{OMIB}}$ ,  $P_{max_{OMIB}}$  and  $\delta_{OMIB}^0$ , respectively. The above-mentioned equations are derived from Equation (4), which is the initial formulation of OMIB motion or swing. All of the parameters given below should be changed into a standard per-unit (p.u.) value to ease calculation in relation to the OMIB.

$$\frac{d^2\delta_{OMIB}}{dt^2} = \pi f_{rated} M^{-1} (P_{m_{OMIB}} - P_{e_{OMIB}}) \quad (4)$$

where

$$P_{m_{OMIB}} = \left(\frac{M_{cm}M_{ncm}}{M_{cm} + M_{ncm}}\right) \left[\left(\frac{1}{M_{cm}}\right) \left(\sum_{n \in cm} P_{m_n}\right) - \left(\frac{1}{M_{ncm}}\right) \left(\sum_{n \in ncm} P_{m_n}\right)\right] \quad (5)$$

$$P_{e_{OMIB}} = \left(\frac{M_{cm}M_{ncm}}{M_{cm} + M_{ncm}}\right) \left[\left(\frac{1}{M_{cm}}\right) \left(\sum_{n \in cm} P_{e_n}\right) - \left(\frac{1}{M_{ncm}}\right) \left(\sum_{n \in ncm} P_{e_n}\right)\right] \quad (6)$$

$P_{m_n}$  is the generating unit's mechanical input power;  $P_{e_n}$  is the real electric power output of generator;  $f_{rated}$  is the rated frequency operated in a system;  $M_{cm}$  is the total inertia for  $cm$  represented by  $\sum_{n \in cm} M_n$ ;  $M_{ncm}$  is the total inertia for  $ncm$  represented by  $\sum_{n \in ncm} M_n$ ; and  $M$  is the OMIB inertia determined by  $2 \times H$ .

- Simultaneously, the OMIB motion or swing equation is simplified by further derivation of Equation (4).

$$\frac{d^2\delta_{OMIB}}{dt^2} = \pi f_{rated} M^{-1} [P_{m_{OMIB}} - [(P_{c_{OMIB}} + P_{max_{OMIB}} \sin(\delta_{OMIB} - v))] \quad (7)$$

where

$$P_{m_{OMIB}} = \frac{M_{ncm} \sum_{n \in cm} P_{m_{cm}} - M_{cm} \sum_{n \in ncm} P_{m_{ncm}}}{M_{cm} + M_{ncm}} \quad (8)$$

$$P_{c_{OMIB}} = \frac{[M_{ncm} E'_{cm}{}^2 G_{cm,cm} - M_{cm} (\sum_{n \in ncm} E'_{ncm}{}^2 G_{ncm,ncm})]}{M_{cm} + M_{ncm}} \quad (9)$$

$$P_{max_{OMIB}} = \sqrt{(C^2 + D^2)} \quad (10)$$

$$v = -\tan^{-1}\left(\frac{C}{D}\right) \quad (11)$$

$$C = \frac{(M_{cm} - M_{ncm}) \sum_{n \in ncm} (E'_{cm})(E'_{ncm}) G_{cm,ncm}}{M_{cm} + M_{ncm}} \quad (12)$$

$$D = \sum_{n \in ncm} E'_{cm} E'_{ncm} G_{cm, ncm} \quad (13)$$

4. In the Transient Stability Assessment (TSA) of a multi-machine, the pre-fault condition is performed to obtain the information of  $P_m$ , generator voltage ( $E'$ ) and shunt conductance ( $G$ ), indispensable for Equations (8)–(13). The  $G$  is originated from the bus admittance matrix of  $Y_{nk}$  constructed without the composition of faulted transmission line and faulted bus. Wherein,  $k$  is the bus number. Simultaneously, Equation (14) is used to determine the OMIB rotor angle during pre-fault condition,  $\delta_{OMIB}^0$ .

$$\delta_{OMIB}^0 = \sin^{-1} \frac{P_{m_{OMIB}}}{P_{max_{OMIB}}} \quad (14)$$

The following section will explain the importance of  $\delta_{OMIB}^0$  for specifying the critical clearing time (CCT) for the tripping of generators and transmission lines.

## 2.2. Determination of Critical Clearing Time for One Machine Connected to an Infinite Bus

Emphasis on the improvement of CCT to corroborate the new changes occurring in a power system is important so that it always operates in a stable condition, especially during the unanticipated fault situation. Duong et al. has discussed a new CCT determination referring to a fault condition occurring in a power system taking into account the operation of wind turbines based squirrel-cage induction generator [21]. Subsequent improvement of CCT has been made to ensure the low voltage ride through type of fault does not infringe the secure operation of a power system connected with the wind turbines based double-fed induction generator [22].

This implies that it is imperative to perform a transient stability analysis, as this is required to stipulate an accurate critical clearing time (CCT) implemented in a protection relay for disconnecting the faulted transmission line so that the healthy system remains transiently stable. During the fault interval, the implication of transmission line tripping is that it will cause a generator to refrain from dispatching its electric power to an infinite bus. As a result, the generator does not provide any electrical output power ( $P_e$ ) and is the reason Equation (4) simplifies to Equation (15). Therefore, Equation (17) is utilized to attain the OMIB critical clearing time,  $t_{c_{OMIB}}$ .

$$\frac{d^2 \delta_{OMIB}}{dt^2} = \frac{\pi f_{rated}}{M} (P_{m_{OMIB}}) \quad (15)$$

Further expansion of Equation (15) yields Equation (16).

$$\delta_{OMIB} = \frac{\pi f_{rated}}{2M} P_{m_{OMIB}} t_{c_{OMIB}}^2 + \delta_{OMIB}^0 \quad (16)$$

Equation (17) is the OMIB critical clearing time ( $t_{c_{OMIB}}$ ) derived from Equation (16). The analytical calculation of  $t_{c_{OMIB}}$  has been proven and discussed thoroughly in [23–25].

$$t_{c_{OMIB}} = \sqrt{\frac{2M(\delta_{crit_{OMIB}} - \delta_{OMIB}^0)}{\pi f_{rated} P_{m_{OMIB}}} \quad (17)$$

where

$$\delta_{crit_{OMIB}} = \cos^{-1} \left( \frac{P_{m_{OMIB}}}{P_{max_{OMIB}}} (\delta_{max_{OMIB}} - \delta_{OMIB}^0) + \cos \delta_{max_{OMIB}} \right) \quad (18)$$

$$\delta_{max_{OMIB}} = 180^\circ - \delta_{OMIB}^0 \quad (19)$$

This signifies that OMIB is further derived to obtain formulation of  $t_{c_{OMIB}}$ . The  $t_{c_{OMIB}}$  based OMIB is useful as a standard reference to specify the CCT for all protection relays in a power system consisting with multi-machine or numerous generators. The importance of OMIB via  $t_{c_{OMIB}}$  towards the power system operating condition comprising multi-machine or numerous generators has also

been discussed and implemented in [24]. Nevertheless, this paper proposes a new approach to analyze the condition of dynamic power system blackout by taking into account the transmission lines and/or generators tripping due to the protection relay operation at the time interval of CCT specified by the  $t_{c_{OMIB}}$  based OMIB. This will be discussed in Section 2.3.

The procedure given below explains in detail the algorithm of the OMIB critical clearing time,  $t_{c_{OMIB}}$ .

1. Perform a fault at the selected bus inflicting the affected transmission line tripping.
2. Execute the TSA so the  $Y_{nk}$  can be determined during the pre-fault and fault conditions.
3. Exert  $E'$  and  $P_m$  in Equation (14) to determine  $\delta_{OMIB}^0$ . The  $Y_{nk}$  obtained in Step (2) is used to determine  $P_m$  during the pre-fault condition.
4. Inflict  $P_{m_{OMIB}}$ ,  $P_{max_{OMIB}}$  and  $\delta_{OMIB}^0$  in Equation (18) to determine  $\delta_{Crit_{OMIB}}$ . The  $P_{m_{OMIB}}$  and  $P_{max_{OMIB}}$  during post-fault condition are attained from Equations (8) and (10), respectively.
5. Use Equation (17) to calculate  $t_{c_{OMIB}}$  for the affected transmission line selected in Step (1);  $t_{c_{OMIB}}$  requires information regarding  $\delta_{OMIB}^0$  and  $\delta_{Crit_{OMIB}}$  as well as  $P_{m_{OMIB}}$ , which is acquired from Steps (7) and (14), respectively. Compute  $t_{c_{OMIB}}$  for the subsequent affected transmission line by repeating Steps (1)–(5).
6. Stipulate a standard CCT by referring to the smallest  $t_{c_{OMIB}}$  and impose it as a reference for all protection relays.

### 2.3. Evaluation of Sensitive Transmission Lines and Total Loading Condition

In a deregulated power system, an inaccurate operation in a protection relay system may cause a proliferation of major system disturbances and eventually lead to a power system blackout [26–28]. This happens because a hidden failure, regarded as an undetected or unidentified defect of a protection relay, causes a false tripping during a normal situation or an exposure to the disturbances from other components in the system [26–28]. The hidden failure probability of  $p_{HF} = 8 \times 10^{-7}$ ,  $p_{HF} = 1 \times 10^{-12}$  and  $p_{HF} = 1 \times 10^{-2}$ , introduced as the three case studies in [29], are subsequently utilized in this section to assess its implication against the probability of dynamic power system blackout. This signifies that the analysis executed based on the proposed approach is contradictory with the analysis undertaken in [29] whereby the probability of static power system blackout is determined based on the three case studies of  $p_{HF}$ . With regards to every case study, the procedure of stochastic event tree will explain in detail the risk assessment by means of average probability of dynamic power system blackout posed by the occurrence of initial transmission line tripping. The information is indispensable for the estimation of severe transmission lines and total loading conditions.

1. Introduce a power system blackout attributed by a stress system condition arising from an increase of 10% on the total loading condition.
2. Specify the  $t_{c_{OMIB}}$  for the entire protection relays as discussed in Section 2.2.
3. Select a transmission line for tripping at an initial event tree,  $i$ . Execute the power flow solution and TSA of multi-machine considering the transmission line tripping at an initial event tree,  $i$ .
4. Determine the probability of incorrect tripping ( $p_{HF}$ ) [30] and forced outage rate ( $FOR$ ) of all exposed transmission lines and exposed generators, respectively. The exposed transmission lines and exposed generators can be described as the system components connected adjacent to the transmission line tripping. The historical information of protection relay hidden failure is used to calculate the  $p_{HF}$  [30]. However, the hidden failure probability of  $p_{HF} = 8 \times 10^{-7}$ ,  $p_{HF} = 1 \times 10^{-12}$  and  $p_{HF} = 1 \times 10^{-2}$  obtained in [29] will be used in the analysis.
5. Randomly or stochastically exert the tripping of exposed transmission lines and/or exposed generators prior to the attainment of  $t_{c_{OMIB}}$  limit imminent in the branch event tree  $j$ . The tripping of exposed transmission lines and exposed generators refer to the randomly or stochastically generated probability that infringe the  $p_{HF}$  limit [30]; and  $FOR$  limit as well as frequency limit or rotor angle limit, respectively.

6. Record the  $p_{HF}$  and  $q_{HF} = 1 - p_{HF}$  of exposed transmission lines, the *FOR* and *1-FOR* of exposed generators and the total random or stochastic tripping,  $Z$ , in the branch event tree  $j$ . The  $q_{HF}$  can be defined as the probability of exposed transmission line not encountering the random tripping event.
7. Use Equation (20) to calculate the conditional probability of tripping ( $P_{Tj}$ ) during branch event tree,  $j$ .

$$P_{Tj} = \prod p_{LGj} \prod q_{LGj} \quad (20)$$

where  $p_{LG}$  is the  $p_{HF}$  for the random or stochastic tripping of exposed transmission lines, or the *FOR* of random or stochastic tripping of exposed generators; and  $q_{LG}$  is the  $q_{HF}$  for non-tripping of exposed transmission lines, or the *1-FOR* of non-tripping of exposed generators.

8. Run the power flow solution and TSA of multi-machine system.
9. Calculate  $P_{Tj}$  using Equation (20) for the ensuing branch event tree  $j$  by repeating Steps (4)–(8).
10. Determine  $P_{C_i}$ , which is the product of tripping probability, using Equation (21).

$$P_{C_i} = \prod_{j=1}^{NJ} P_{Tj} \quad (21)$$

11. Determine  $\bar{P}_{C_i}$ , which is the average probability of sequential random or stochastic tripping, using Equation (22) by repeating Steps (4)–(10) for  $KP = 1000$  times.

$$\bar{P}_{C_i} = \frac{1}{KP} \sum_{kp=1}^{KP} P_{C_i, kp} \quad (22)$$

12. Acquire  $\bar{P}_{C_i}$  for the subsequent tripping of transmission line at initial event tree,  $i$ , by executing Steps (3)–(11).
13. Execute Steps (1)–(15) to determine  $\bar{P}_{C_i}$  for every increment of total loading condition until its maximum level is reached.
14. Calculate  $\mu(\bar{P}_{C_i})$ , which is the estimated average probability of dynamic power system blackout, using Equation (23).

$$\mu(\bar{P}_{C_i}) = \frac{1}{L} \sum_{l=1}^L \bar{P}_{C_i, l} \quad (23)$$

where  $L$  is the total steps required for the increase of total loading condition.

15. Distinguish the sensitive transmission lines during the initial tripping or initial event tree by means of significant increase in the  $\mu(\bar{P}_{C_i})$  value.
16. Calculate  $\mu(\bar{P}_{C_i})$ , which is the estimated average probability of dynamic power system blackout, using Equation (24).

$$\mu(\bar{P}_{C_i}) = \frac{1}{I} \sum_{i=1}^I \bar{P}_{C_i, i} \quad (24)$$

where  $I$  is the total number of transmission lines.

17. Arrange the  $\mu(\bar{P}_{C_i})$  in ascending order to determine the critical dynamic power system blackout that is caused by the severity of total loading condition. Distinguish the severity of total loading conditions inflicting a critical dynamic power system blackout by means of significant increase in the  $\mu(\bar{P}_{C_i})$  value.

### 3. Results

This section will discuss the sustainability of power system operation for the case studies of IEEE RTS-79 and IEEE RTS-96 under the perspective of risk assessment in dynamic power system blackout. IEEE RTS-79 and IEEE RTS-96 were designed based on the real parameters and pragmatic components acquired based on consensus from power system experts. Usually, these systems are used

as a case study for benchmarking the findings of similar study obtained based on different methods or approaches suggested by researchers. Similarly, the initiative highlighted in this manuscript is the implementation of IEEE RTS-79 and IEEE RTS-96 as case studies, which is sufficient to prove the proposed method can be used to determine the risk of dynamic system blackout in a real power system. There are 13 load buses, 11 generator buses and 38 transmission lines for the case study of IEEE RTS-79, as shown in Figure 1 [31]. There are 40 load buses, 120 transmission lines and 33 generator buses for the case study of IEEE RTS-96, as shown in Figure 2 [32]. To obtain accurate results, comparative results were conducted based on the risk assessment of dynamic and static [29,33] power system blackout subject to the three cases of relay hidden failure.

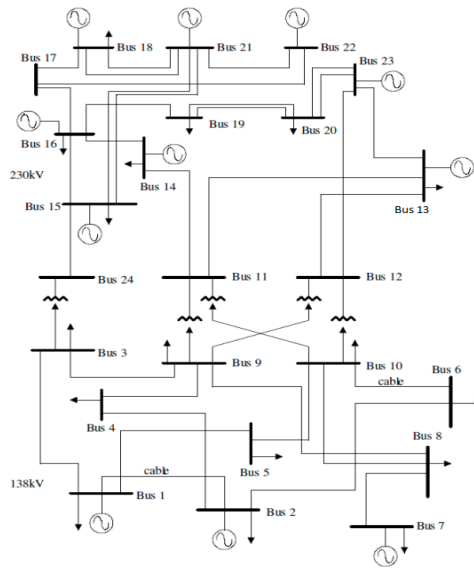


Figure 1. A single line diagram of the IEEE RTS-79 system.

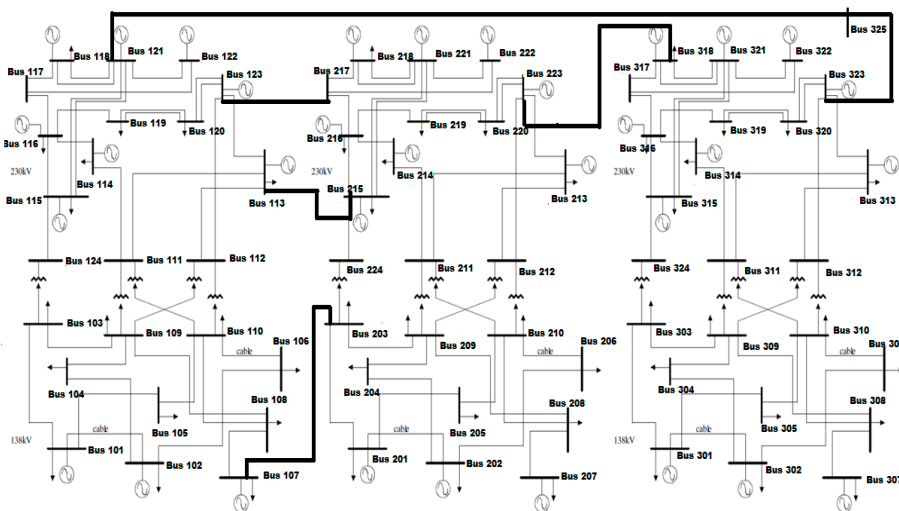


Figure 2. A single line diagram of the IEEE RTS-96 system.

### 3.1. The Impact of Hidden Failure in Protection System towards the Risk Assessment of Dynamic Power System Blackout

In this section, the sustainability of the power system operating condition will be discussed referring to the risk assessment of dynamic power system blackout,  $\mu(\bar{P}_{C_i})$ , based on the hidden failure probabilities of  $p_{HF} = 1 \times 10^{-12}$ ,  $p_{HF} = 8 \times 10^{-7}$  and  $p_{HF} = 1 \times 10^{-2}$ . The procedure used to

perform the risk assessment of the dynamic power system blackout is discussed in Section 2.3. The risk assessment of dynamic power system blackout is divided into two main sections, with the first analysis deployed to determine the sensitivity of the transmission lines, taking into account the effect of hidden failure in a protective relay system. This is followed by the assessment of critical total system loading condition in tandem with the risk of dynamic power system blackout.

The initial transmission line tripping for both systems is performed based on the operation of protection relays at the CCT of 0.01 s. The CCT is acquired from the lowest  $t_{COMIB}$  of all the transmission line outages determined based on the concept that is discussed in Section 2.2. The lowest  $t_{COMIB}$  is well suited to be used as a reference for setting the CTT applied to all of the protective relays to ensure stability in the transient response of rotor angle for all generators ( $\delta_g$ ) in conjunction with the initial tripping of any transmission line. It contradicts the CCT assigned based on the time beyond the lowest  $t_{COMIB}$ , which may cause an unstable transient response of  $\delta_g$  subsequent to the initial tripping of a particular transmission line. Therefore, for the case study of IEEE RTS-79, the initial tripping of line 1–3 and line 1–5 give the lowest  $t_{COMIB}$  of 0.01 s, which will be used as a reference in setting the standard CCT for all protection relays. Figure 3a shows one of the results taken as an example to attest that the initial tripping of line 1–3 at CCT = 0.01 s will lead to a stable transient response of  $\delta_g$ . This contradicts the unstable transient response of  $\delta_g$  that happened due to the CCT of 0.02 s specified above its standard limit for the initial tripping of line 1–3, as shown in Figure 3b.

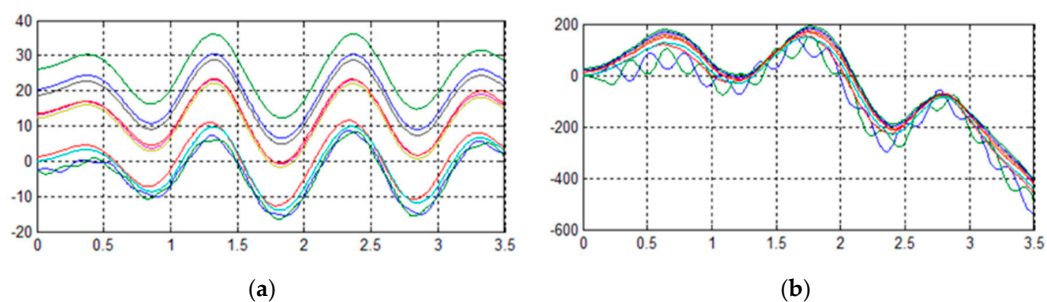


**Figure 3.** Transient response of  $\delta_g$  subsequent to the initial tripping of line 1–3: (a) CCT specified based on the lowest  $t_{COMIB}$  of 0.01 s; and (b) CCT specified based on the  $t_{COMIB}$  of 0.02 s.

A similar situation also applies to the case study of IEEE RTS-96, in which all of the protection relays are set with the standard CCT of 0.01 s, which is the lowest  $t_{COMIB}$  that occurred during the initial tripping of line 101–103, line 101–105, line 201–202, line 201–203, line 301–305 and line 302–304. This can be observed via one of the results taken as an example in which the initial tripping of line 101–103 at CCT = 0.01 s may cause a stable transient response of  $\delta_g$ , as shown in Figure 4a. Setting the CCT to a non-standard limit of 0.02 s for the initial tripping of line 101–103 has an adverse impact on the system resulting in unstable transient response of  $\delta_g$ , as shown in Figure 4b.

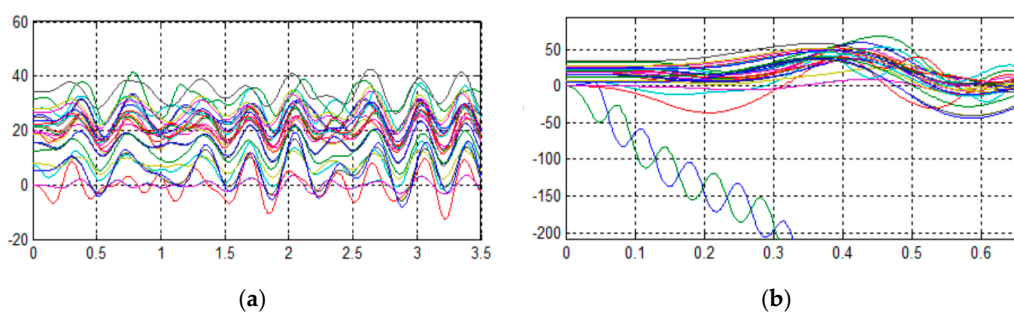


**Figure 4.** Transient response of  $\delta_g$  subsequent to the initial tripping of line 101–103: (a) CCT specified based on the lowest  $t_{COMIB}$  of 0.01 s; and (b) CCT specified based on the  $t_{COMIB}$  of 0.02 s.

Figure 5 shows the results of  $\mu(\bar{P}_{C_i})$  for each initial sensitive transmission line tripping at three different cases of relay hidden failure for IEEE RTS-79. However, the results shown in Figure 5 only depict selected sensitive initial transmission line tripping that have large values of  $\mu(\bar{P}_{C_i})$ . For all three case studies, the  $\mu(\bar{P}_{C_i})$  is arranged to specify the sensitive transmission lines that have a significant contribution to a critical dynamic power system blackout. The discussion emphasizes the relatively large value of  $\mu(\bar{P}_{C_i})$  that signifies the chosen initial transmission line tripping is sensitive to the dynamic system operating condition causing to the occurrence of critical dynamic power system blackout. In the figure, it is observed that the value of  $\mu(\bar{P}_{C_i})$  for the case of  $p_{HF} = 1 \times 10^{-12}$  is higher than the cases where  $p_{HF} = 8 \times 10^{-7}$  and  $p_{HF} = 1 \times 10^{-2}$ . It is noted in Section 2.3 that the historical information of power system blackout provides the inherent  $p_{HF}$  value of  $8 \times 10^{-7}$ , which has the lowest  $\mu(\bar{P}_{C_i})$  value for the majority of sensitive initial transmission lines tripping. This result implies that accurate estimation of hidden failure probability has a significant impact on the result of risk assessment in dynamic power system blackout.

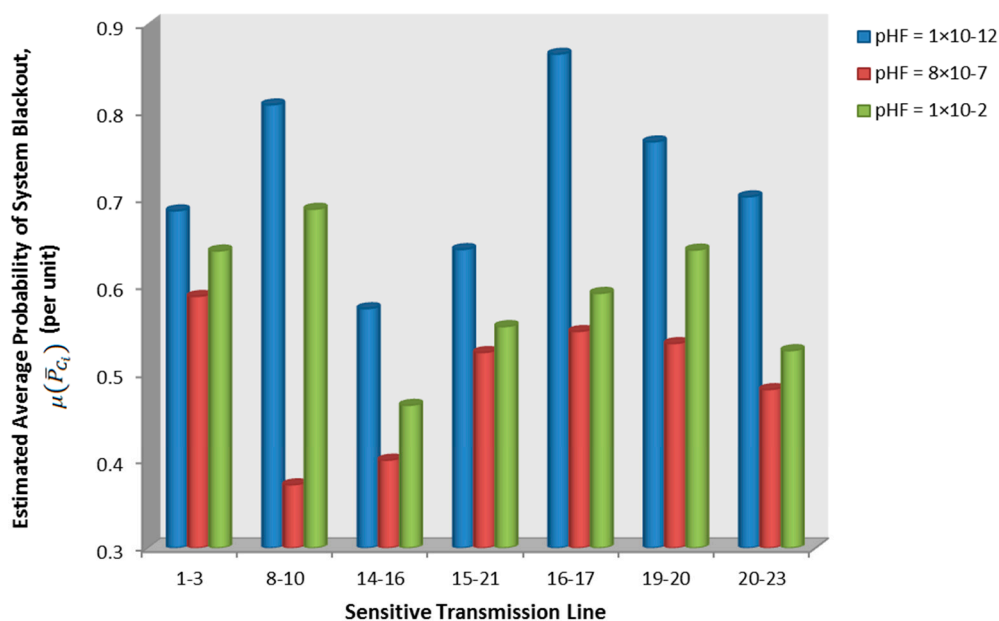


Figure 5. Sensitive initial transmission line tripping obtained based on the  $\mu(\bar{P}_{C_i})$  for the IEEE RTS-79.

Figure 6 presents the tabulation of selected sensitive transmission lines arranged according to the risk assessment of dynamic power system blackout,  $\mu(\bar{P}_{C_i})$ . According to [32], IEEE RTS-96 comprises 120 transmission lines. Nevertheless, similar to the aforementioned analysis, the selected results of sensitive initial transmission lines refer to the largest risks of dynamic power system blackout,  $\mu(\bar{P}_{C_i})$ . Similar to the above analysis, the risk based  $\mu(\bar{P}_{C_i})$  of dynamic power system blackout for IEEE RTS-96 is analyzed under three types of relay hidden failure. The findings are similar to the analysis shown above in Figure 5, where there is significant difference of risk based  $\mu(\bar{P}_{C_i})$  between each initial tripping of sensitive transmission line. However, the case of  $p_{HF} = 1 \times 10^{-2}$  causes all sensitive transmission lines to acquire  $\mu(\bar{P}_{C_i})$  that is higher than the  $\mu(\bar{P}_{C_i})$  of  $p_{HF} = 8 \times 10^{-7}$  and  $p_{HF} = 1 \times 10^{-12}$ . Nevertheless, the exact value for the case of  $p_{HF} = 8 \times 10^{-7}$  brings the same conclusion: the  $\mu(\bar{P}_{C_i})$  can be regarded as low for IEEE RTS-96, as depicted in Figure 6, which is similar to the IEEE RTS-79 (Figure 5). This signifies that determination of the exact value of hidden failure probability plays an important role, since it will render the right conjecture with an accurate result in the risk assessment of dynamic power system blackout.

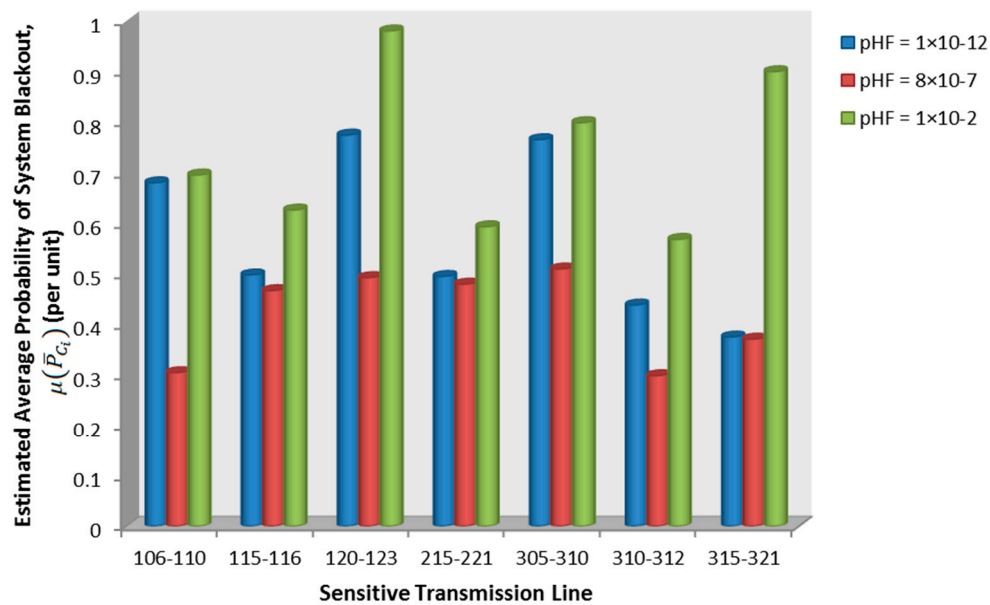


Figure 6. Sensitive initial transmission line tripping obtained based on the  $\mu(\bar{P}_{C_i})$  for the IEEE RTS-96.

### 3.2. Comparison of Sensitive Transmission Lines Tripping Associated with the Static and Dynamic Power System Blackouts

This section will discuss the comparison of the sensitive initial transmission lines tripping corresponding to the risk based  $\mu(\bar{P}_{C_i})$  of static [29,33] and dynamic power system blackouts. IEEE RTS-79 and IEEE RTS-96 are used as the case studies for comparison of the sensitive transmission lines tripping, as depicted in Figures 7 and 8, respectively.

Figure 7 represent the comparison of sensitive initial transmission lines tripping with respect to the risk assessment of static and dynamic power system blackouts for the case study of IEEE RTS-79. In relation to the static power system blackout,  $p_{HF} = 8 \times 10^{-7}$  causes the sensitive initial transmission line tripping to have a  $\mu(\bar{P}_{C_i})$  that is higher than the  $p_{HF} = 1 \times 10^{-12}$  and  $p_{HF} = 1 \times 10^{-2}$  cases. The  $p_{HF} = 1 \times 10^{-2}$  case confers the lowest  $\mu(\bar{P}_{C_i})$  value, for almost all of the sensitive initial transmission lines tripping related to the case of static power system blackout. Contradictorily, with  $\mu(\bar{P}_{C_i})$ , in the case of dynamic power system blackout,  $p_{HF} = 1 \times 10^{-12}$  causes all of the sensitive initial transmission lines tripping to obtain a  $\mu(\bar{P}_{C_i})$  that is higher than the  $\mu(\bar{P}_{C_i})$  of the  $p_{HF} = 8 \times 10^{-7}$  and  $p_{HF} = 1 \times 10^{-2}$  cases. The  $p_{HF} = 8 \times 10^{-7}$  case exerts to the lowest  $\mu(\bar{P}_{C_i})$  for all of the initial sensitive line tripping for the case of dynamic power system blackout. Comparative studies show that the  $p_{HF} = 8 \times 10^{-7}$  case causes the highest  $\mu(\bar{P}_{C_i})$  value for all initial sensitive lines tripping under the static power system blackout case study. The results contradict the outcomes acquired from the dynamic power system blackout case studies in that the highest  $\mu(\bar{P}_{C_i})$  value for all of the initial sensitive transmission lines tripping are attained subject to the  $p_{HF} = 1 \times 10^{-12}$  case. Therefore, for the case study of static power system blackout,  $p_{HF} = 1 \times 10^{-2}$  causes the lowest  $\mu(\bar{P}_{C_i})$  value for all of the initial sensitive transmission lines tripping. This contrasts with the dynamic power system blackout case study in which the lowest  $\mu(\bar{P}_{C_i})$  is imposed by  $p_{HF} = 8 \times 10^{-7}$ . These results highlight that the dynamic power system blackout has a tangible impact, causing a large value of  $\mu(\bar{P}_{C_i})$  for all of the initial sensitive transmission lines tripping as compared to the impact of static power system blackout. The results also imply that uncertain tripping of the exposed generator as well as the exposed transmission line may cause a worse condition due to considerable risk in the power system operation originated from the dynamic power system blackout.

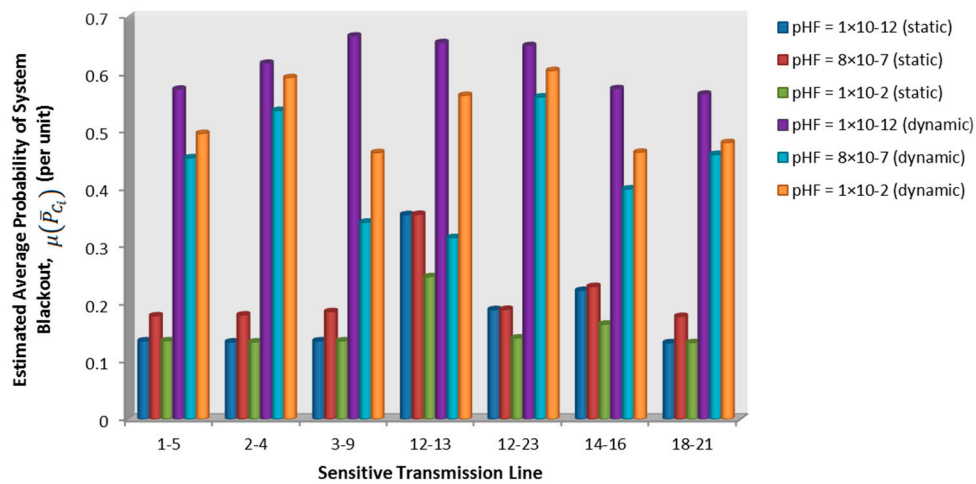


Figure 7. Comparison of risk based  $\mu(\bar{P}_{C_i})$  under the case study of IEEE RTS-79.

Comparison of the  $\mu(\bar{P}_{C_i})$  values obtained based on the case of static and dynamic power system blackout is also performed on the IEEE RTS-96 test system, as shown in Figure 8. Similar to the above-mentioned discussion for the case study of IEEE RTS-79, in relation to the occurrence of static power system blackout, it is obvious that  $p_{HF} = 8 \times 10^{-7}$  and  $p_{HF} = 1 \times 10^{-12}$  give similar results for  $\mu(\bar{P}_{C_i})$ . In addition, the results also have shown that the  $p_{HF} = 1 \times 10^{-2}$  case causes the sensitive initial transmission line tripping to have a  $\mu(\bar{P}_{C_i})$  that is lower than the  $p_{HF} = 1 \times 10^{-12}$  and  $p_{HF} = 8 \times 10^{-7}$  cases. On the other hand, the  $p_{HF} = 1 \times 10^{-12}$  case exerts the highest  $\mu(\bar{P}_{C_i})$  for all of the sensitive initial transmission lines tripping, subject to the occurrence of static power system blackout. Under the perspective of dynamic power system blackout,  $p_{HF} = 1 \times 10^{-2}$  causes the highest value of  $\mu(\bar{P}_{C_i})$  for most of the initial sensitive line trippings compared to the  $p_{HF} = 1 \times 10^{-12}$  and  $p_{HF} = 8 \times 10^{-7}$  cases. Contradictory to the results of  $\mu(\bar{P}_{C_i})$  that can be observed for the case of dynamic power system blackout, the  $p_{HF} = 8 \times 10^{-7}$  case causes most of the sensitive transmission lines to obtain a  $\mu(\bar{P}_{C_i})$  that is lower than the  $\mu(\bar{P}_{C_i})$  of  $p_{HF} = 1 \times 10^{-12}$  and  $p_{HF} = 1 \times 10^{-2}$  cases. From the results shown in Figure 8, a large value of  $\mu(\bar{P}_{C_i})$ , for all of the initial transmission lines tripping that cause a worse power system operating condition, is attained, corresponding to the dynamic power system blackout in contrast with the impact of static power system blackout.

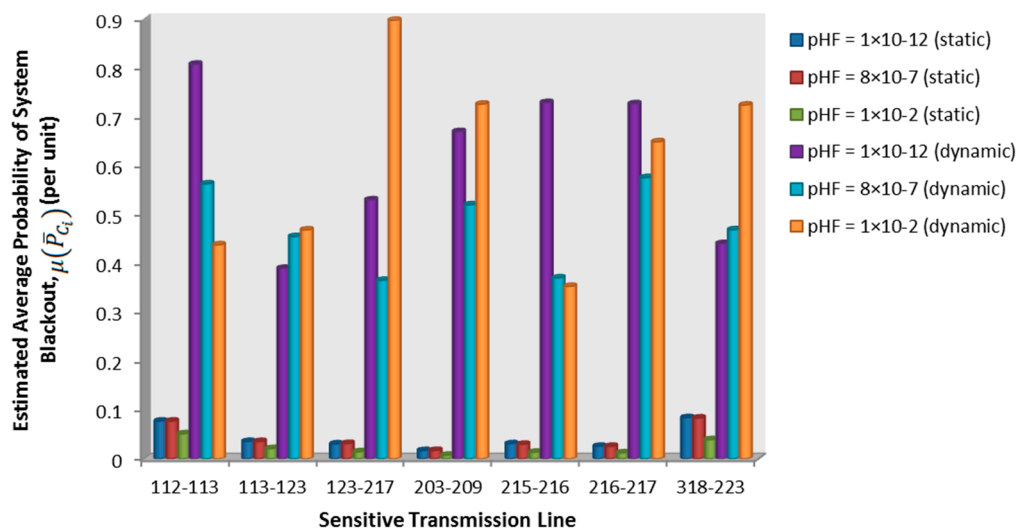


Figure 8. Comparison of risk based  $\mu(\bar{P}_{C_i})$  for the case study of IEEE RTS-96.

The occurrence of dynamic power system blackout may cause a worse power system operating condition because of a  $\mu(\bar{P}_{C_i})$  that is larger, as compared to the results obtained based on the static power system blackout. Despite this, it is important to perform a dynamic power system blackout, which has a significant impact on the risk assessment of a power system operation.

Albeit, for both case studies, the risk of dynamic power system blackout is greater than the risk of static power system blackout, as depicted in Figures 7 and 8. However, a significant difference in terms of its range in the risk of static power system blackout can be observed by comparing the results obtained from IEEE-RTS79 and IEEE-RTS69 given in Figures 7 and 8, respectively. It can be assumed that this problem stems from the transmission line outage solely considered as the tripping parameter performed in the procedure of static power system blackout. This may cause a lower and inconsistent range in the risk of static power system blackout, which can be observed via the comparison of results obtained from the IEEE RTS-79 and IEEE-RTS-96. Therefore, it is imperative to take into account the critical parameters of transmission line, generator rotor angle and frequency generator, which will significantly affect the power system operating condition, to provide more accurate results with higher and consistent range for the risk of dynamic power system blackout system observed through the comparison between the IEEE RTS-79 and IEEE RTS-96.

### 3.3. Determination of Severe Total Loading Condition Based on the Risk of Dynamic Power System Blackout

The determination of severe total loading condition is performed by referring to the risk based  $\mu(\bar{P}_{C_i})$  of critical dynamic power system blackout. It is worth noting that the three case studies originate from [29], and are further explored for in-depth analysis of the proposed approach that will be discussed in this section. Figure 9 shows the results of  $\mu(\bar{P}_{C_i})$  representing the risk of dynamic power system blackout attributed to a 150–240% increased of total loading condition taking into account three different types of  $p_{HF}$ . The beginning of system operating risk for the IEEE RTS-79 arises during 150% increase of total loading condition. The severity of dynamic power system blackout starts to appear at 160% increase of total loading condition. The results are obtained based on the three cases of  $p_{HF} = 8 \times 10^{-7}$ ,  $p_{HF} = 1 \times 10^{-12}$  and  $p_{HF} = 1 \times 10^{-2}$ . A significant increase of  $\mu(\bar{P}_{C_i})$  can be seen for all the three case studies, when there is beyond 160% increased of total loading condition. From the three different case studies,  $p_{HF} = 1 \times 10^{-2}$  is causing to the most critical condition in the risk assessment compared to the  $\mu(\bar{P}_{C_i})$  obtained based on  $p_{HF} = 1 \times 10^{-12}$  and  $p_{HF} = 8 \times 10^{-7}$  cases.

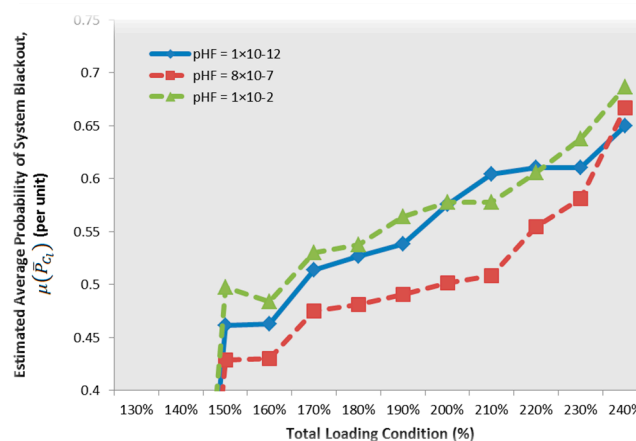


**Figure 9.** The implication of total loading condition increment towards the risk based  $\mu(\bar{P}_{C_i})$  for the case study of dynamic power system blackout in an IEEE RTS-79.

The results have shown that determination of an accurate  $p_{HF}$  value is important, notably when there is a severe increase of total loading condition causing to a significant impact on the emergence of critical dynamic power system blackout. The historical information of power system blackout provides

the inherent  $p_{HF}$  value of  $8 \times 10^{-7}$ , which has the lowest  $\mu(\bar{P}_{C_i})$  value at every total loading condition. The results signify the importance of determining the risk of dynamic power system blackout that takes into account the accurate estimation of hidden failure probability values considering the historical information of power system blackouts.

The above-mentioned discussion is similar to the result of risk based  $\mu(\bar{P}_{C_i})$  in determining the critical dynamic power system blackout for the IEEE RTS-96. Figure 10 shows a rapid increase for the results of risk based  $\mu(\bar{P}_{C_i})$  with the 130–220% increase of total loading condition. In the case study of IEEE RTS-96, the risk of system operating condition starts to emerge when the total system loading condition is increased by 130%. By referring to the three types of  $p_{HF}$ , the system begins to experience a critical dynamic power system blackout as the total loading condition is severely increased above 140%. It is noticeable that the value of  $\mu(\bar{P}_{C_i})$  starts to increase in conjunction with a 140% of total loading condition. This refers to  $p_{HF} = 1 \times 10^{-12}$  inflicting the largest amount of  $\mu(\bar{P}_{C_i})$  in contrast with the risk acquired via the  $p_{HF} = 8 \times 10^{-7}$  and  $p_{HF} = 1 \times 10^{-2}$ . Albeit the lowest  $\mu(\bar{P}_{C_i})$  value incurred for all of the increased total loading conditions with  $p_{HF} = 8 \times 10^{-7}$ , it is still important to record the historical information of power system blackout so that the hidden failure probability of  $p_{HF} = 8 \times 10^{-7}$  is accurately determined, which is indispensable for the risk assessment of dynamic power system blackout.

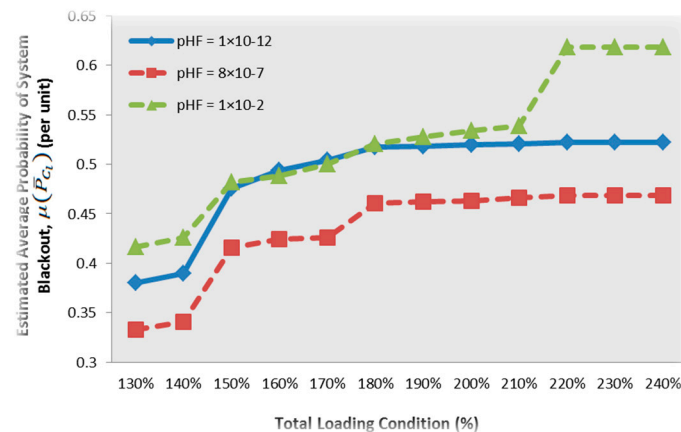


**Figure 10.** Implication of total loading condition into against the risk based  $\mu(\bar{P}_{C_i})$  for the case study of dynamic power system blackout in an IEEE RTS-96.

The results related to the  $\mu(\bar{P}_{C_i})$  for the case study of RTS-79 and IEEE RTS-96 implies that inaccurate value of  $p_{HF}$  will adversely affect the result of critical dynamic power system blackout adversely afflicted by the severe total loading condition. The inherent value of  $p_{HF} = 8 \times 10^{-7}$  obtained from the historical information of power system blackout results in the lowest risk based  $\mu(\bar{P}_{C_i})$  of dynamic power system blackout for both test systems. Therefore, it is important for the power marketers and utilities to identify the correct value of  $p_{HF}$ , which significantly impacts the severely increased total loading condition against the emergence of critical dynamic power system blackout. Besides that, marketers and utilities will encounter ineffective electricity trading as this consequence is caused by inaccurate estimation of dynamic power system blackout disrupted by the discrepancies of  $p_{HF}$  value.

#### 3.4. Comparison of Severe Total Loading Condition under the Perspective of Static and Dynamic Power System Blackouts

This section explains the comparative results of severe total loading condition obtained corresponding to the static [29,33] and dynamic power system blackouts for IEEE RTS-79 and IEEE RTS-96. Figure 11 depicts the results of  $\mu(\bar{P}_{C_i})$ , which represents the severity of total loading condition

for static and dynamic power system blackouts with regard to the implication of protection system hidden failure for the case study of IEEE RTS-79.

In conjunction with the case study of static power system blackout, it is observed that  $p_{HF} = 8 \times 10^{-7}$  and  $p_{HF} = 1 \times 10^{-2}$  produce similar high values of risk based  $\mu(\bar{P}_{C_i})$  for most increments of the total loading conditions, followed by  $p_{HF} = 1 \times 10^{-12}$ . Contradictory to the results of  $\mu(\bar{P}_{C_i})$  adversely implicated by the dynamic power system blackout,  $p_{HF} = 8 \times 10^{-7}$  produces the lowest risk based  $\mu(\bar{P}_{C_i})$  for every increment of total loading condition in comparison to  $p_{HF} = 1 \times 10^{-2}$  and  $p_{HF} = 1 \times 10^{-12}$ . The comparative studies emphasize that  $p_{HF} = 8 \times 10^{-7}$  causes the largest  $\mu(\bar{P}_{C_i})$  value corresponding to the case study of static power system blackout. This conflicts with the results obtained based on the case study of dynamic power system blackout that  $p_{HF} = 8 \times 10^{-7}$  causes the lowest value of  $\mu(\bar{P}_{C_i})$ . For all the three cases of  $p_{HF}$ , it is obvious that the  $\mu(\bar{P}_{C_i})$  of total loading condition is rather small for the static power system blackout. On the other hand, the total loading condition and dynamic power system blackout severely cause relatively large value of  $\mu(\bar{P}_{C_i})$  in the power system operation. Therefore, it is worth noting that uncertainty in the exposed generator and exposed transmission line tripping, compounded with the rapid increased of total loading condition above 140%, will severely aggravate the implication of dynamic power system blackout.

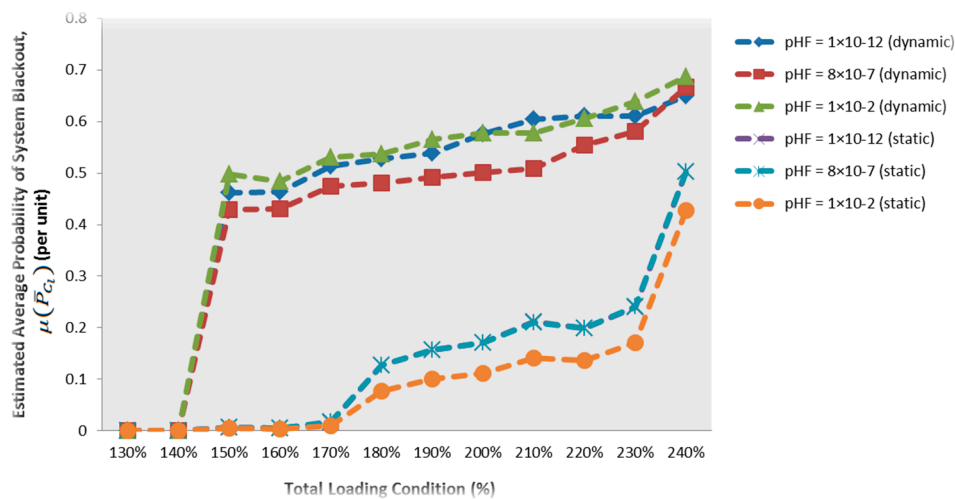


**Figure 11.** Significance of static and dynamic power system blackout to the risk based  $\mu(\bar{P}_{C_i})$  for the case study of for IEEE RTS-79.

With regards to the case study of IEEE RTS-96, comparative study based on the results of  $\mu(\bar{P}_{C_i})$  is performed to distinguish significant deterioration in the power system operation originated either from the static or dynamic power system blackouts afflicted by the hidden failure compounded with the severe total loading condition, as shown in Figure 12. By referring to the results of  $\mu(\bar{P}_{C_i})$  obtained in accordance with the static power system blackout,  $p_{HF} = 1 \times 10^{-12}$  and  $p_{HF} = 8 \times 10^{-7}$  produce similar results for  $\mu(\bar{P}_{C_i})$ , which are higher than the value of  $\mu(\bar{P}_{C_i})$  for  $p_{HF} = 1 \times 10^{-2}$ . On the other hand, for the dynamic power system blackout,  $p_{HF} = 8 \times 10^{-7}$  produces the lowest risk based  $\mu(\bar{P}_{C_i})$  for every increment of total loading condition followed by  $p_{HF} = 1 \times 10^{-12}$  and  $p_{HF} = 1 \times 10^{-2}$ .

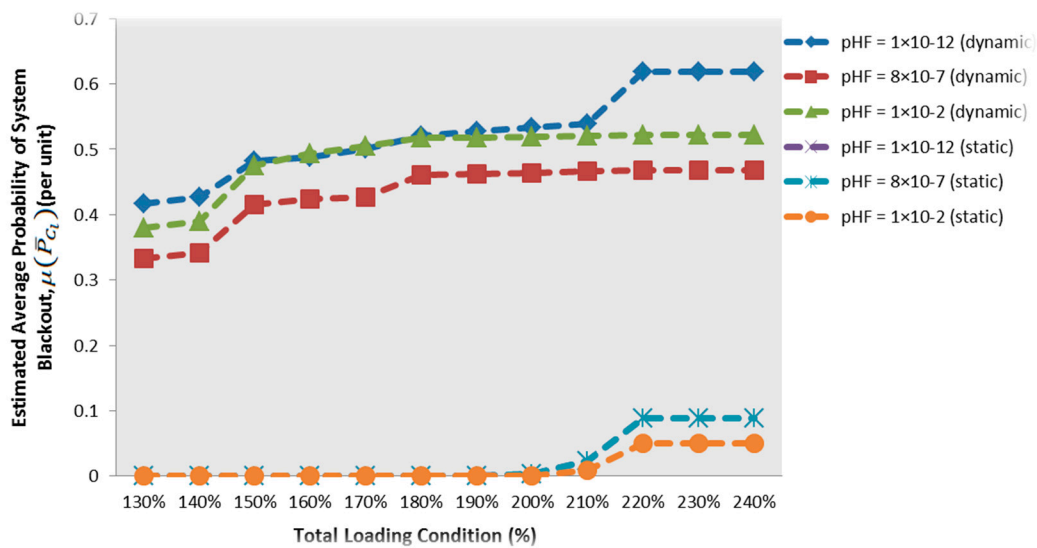


**Figure 12.** Significance of static and dynamic power system blackout to the risk based  $\mu(\bar{P}_{C1})$  for the case study of IEEE RTS-96.

In the case study of IEEE RTS-96, the results divulge the largest  $\mu(\bar{P}_{C1})$  value incurred by  $p_{HF} = 8 \times 10^{-7}$  during the case study of static power system blackout. Conversely, in the case of dynamic power system blackout,  $p_{HF} = 8 \times 10^{-7}$  causes the lowest  $\mu(\bar{P}_{C1})$  for every total loading condition increment. For all three cases of  $p_{HF}$ , it is obvious that the  $\mu(\bar{P}_{C1})$  of total loading condition is rather small for the static power system blackout. However, the dynamic power system blackout produces relatively large value of  $\mu(\bar{P}_{C1})$  for the total loading condition. Therefore, this implies that a severe power system operating condition is exacerbated due to the occurrence of dynamic power system blackout emanating from the uncertainty of exposed generator and exposed transmission lines tripping, compounded by the rapid increase of total loading condition above 130%. Similar to the findings discussed above in relation to Figure 11, the results shown in Figure 12 attest that the dynamic power system blackout undertaken according to the three case studies of  $p_{HF}$  yield a considerably large value of  $\mu(\bar{P}_{C1})$  compared to the results obtained based on the static power system blackout. This is because the overloaded transmission line, dynamic violation of generator rotor angle limit and dynamic violation of generator frequency limit are additional limitations of power system parameters considered in the procedure of the dynamic power system blackout that is discussed in Section 2.3.

#### 4. Conclusions

This study developed a new framework of stochastic event tree used for sustainability assessment in a power system operation pertaining to the impact of dynamic power system blackout. In depth analysis has been carried out based on two types of risk assessment in power system operating condition, static and dynamic power system blackouts, customarily caused by disoperation or hidden failure of a protection system. The obtained results imply that it is important to determine a realistic value in the probability of hidden value, which is  $p_{HF} = 8 \times 10^{-7}$ , as it gives a higher risk of dynamic power system blackout. Comparative studies conducted between two types of risk assessment in system operating conditions signify that the dynamic power system blackout confers a higher risk in contrast to the static power system blackout. This is because the dynamic power system blackout was designed by means of propagation in the exposed power system component tripping attributed by the overloaded transmission line, violation of generator rotor angle limit or intrusion of generator frequency limit. This contradicts the insignificant result of static power system blackout that solely takes into account the propagation tripping of overloaded transmission line as the violation of steady state system operating constraint. In addition, by utilizing the proposed stochastic event tree technique

for risk assessment of dynamic power system blackout, it is beneficial and useful to utility and power system planners because of its robustness to identify the sensitive transmission lines and severity of total loading conditions that have the potential to cause critical dynamic power system blackouts. Eventually, pragmatic implementation of the proposed concept will assist utility and power system planners to stipulate the best action to avert problems related to the sustainable power system operating condition.

**Acknowledgments:** This research project is undertaken under the auspices of research grants FRGS/2/2014/TK03/UITM/02/1, RAGS/1/2014/TK03/UITM//6, 600-RMI/DANA 5/3/LESTARI (77/2015) and 600-IRMI/DANA/5/3/BESTARI(0001/2016) conferred by the Ministry of Higher Education (MOHE), Malaysia and the Institute of Research Management & Innovation (IRMI), Universiti Teknologi MARA, Malaysia.

**Author Contributions:** All of the authors have participated in the preparation of the manuscript. Muhammad Murtadha Othman and Ismail Musirin participated in initial discussion for deciding the methodology used for solving the problems. Muhammad Murtadha Othman and Nur Ashida Salim devised the experiments. Nur Ashida Salim performed all the simulation work, gathered important results and drafted the article. Ismail Musirin helped interpret the data and results. The main revisions were done by all of the authors before finalizing the manuscript.

**Conflicts of Interest:** The authors declare no conflict of interest.

## References

1. Aghamohammadi, M.R.; Hashemi, S.; Hasanzadeh, A. A new approach for mitigating blackout risk by blocking minimum critical distance relays. *Int. J. Electr. Power Energy Syst.* **2016**, *75*, 162–172. [[CrossRef](#)]
2. Belkacemi, R.; Bababola, A.; Zarrabian, S.; Craven, R. Multi-agent system algorithm for preventing cascading failures in smart grid systems. In Proceedings of the North American Power Symposium (NAPS), Pullman, WA, USA, 7–9 September 2014.
3. Li, Y.F.; Sansavini, G.; Zio, E. Non-dominated sorting binary differential evolution for the multi-objective optimization of cascading failures protection in complex networks reliability. *Eng. Syst. Saf.* **2013**, *111*, 195–205. [[CrossRef](#)]
4. Scala, A.; Lucentini, P.G.D.S.; Caldarelli, G.; D’Agostino, G. Cascades in interdependent flow networks. *Phys. D Nonlinear Phenom.* **2016**, *323*, 35–39. [[CrossRef](#)]
5. Scala, A.; Lucentini, P.G.D.S. The equal load-sharing model of cascade failures in power grids. *Phys. A Stat. Mech. Appl.* **2016**, *462*, 737–742. [[CrossRef](#)]
6. Ke, S.; Zhen-Xiang, H. Analysis and comparison on several kinds of models of cascading failure in power system. In Proceedings of the 2005 IEEE/PES Transmission and Distribution Conference and Exhibition: Asia and Pacific, Dalian, China, 18 August 2005.
7. Zhou, B.; Li, R.; Cheng, L. A risk assessment model of power system cascading failure considering the impact of ambient temperature. In Proceedings of the 2014 Asia-Pacific Conference on Electronics and Electrical Engineering, Shanghai, China, 27–28 December 2015.
8. Henneaux, P.; Song, J.; Cotilla-Sanchez, E. Dynamic probabilistic risk assessment of cascading outages. In Proceedings of the 2015 IEEE Power & Energy Society General Meeting, Denver, CO, USA, 26–30 July 2015.
9. Henneaux, P.; Labeau, P.E.; Maun, J.C.; Haarla, L. A two-level probabilistic risk assessment of cascading outages. *IEEE Trans. Power Syst.* **2016**, *31*, 2393–2403. [[CrossRef](#)]
10. Henneaux, P.; Labeau, P.E.; Maun, J.C. A level-1 probabilistic risk assessment to blackout hazard in transmission power systems. *Reliab. Eng. Syst. Saf.* **2012**, *102*, 41–52. [[CrossRef](#)]
11. Xue, Y.; Van Cutsem, T.; Ribbens-Pavella, M. Extended equal area criterion justifications, generalizations, applications. *IEEE Trans. Power Syst.* **1989**, *4*, 44–52. [[CrossRef](#)]
12. Xue, Y.; Van Cutsem, T.; Ribbens-Pavella, M. A simple direct method for fast transient stability assessment of large power systems. *IEEE Trans. Power Syst.* **1998**, *3*, 400–412. [[CrossRef](#)]
13. Bhat, S.; Glavic, M.; Pavella, M.; Bhatti, T.S.; Kothari, D.P. A transient stability tool combining the SIME method with MATLAB and SIMULINK. *Int. J. Electr. Eng. Educ.* **2006**, *43*, 119–133. [[CrossRef](#)]
14. Pizano-Martínez, A.; Fuerte-Esquivel, C.R.; Zamora-Cárdenas, E.; Ruiz-Vega, D. Selective transient stability-constrained optimal power flow using a SIME and trajectory sensitivity unified analysis. *Electr. Power Syst. Res.* **2014**, *109*, 32–44. [[CrossRef](#)]

15. Busan, S. Dynamic Available Transfer Capability Calculation Considering Generation Rescheduling. Master's Thesis, Universiti Teknologi MARA, Shah Alam, Malaysia, September 2012.
16. Busan, S.; Othman, M.M.; Musirin, I.; Mohamed, A.; Hussain, A. A new algorithm for the available transfer capability determination. *Math. Probl. Eng.* **2010**, *2010*, 795376. [[CrossRef](#)]
17. Li, Y.H.; Yuan, W.P.; Chan, K.W.; Liu, M.B. Coordinated preventive control of transient stability with multi-contingency in power systems using trajectory sensitivities. *Int. J. Electr. Power Energy Syst.* **2011**, *33*, 147–153. [[CrossRef](#)]
18. Yuan, Y.; Kubokawa, J.; Sasaki, H. A solution of optimal power flow with multicontingency transient stability constraints. *IEEE Trans. Power Syst.* **2003**, *18*, 1094–1102. [[CrossRef](#)]
19. Xia, Y.; Chan, K.W. Dynamic constrained optimal power flow using semi-infinite programming. *IEEE Trans. Power Syst.* **2006**, *21*, 1455–1457. [[CrossRef](#)]
20. Pizano-Martianez, A.; Fuerte-Esquivel, C.R.; Ruiz-Vega, D. Global transient stability-constrained optimal power flow using an OMIB reference trajectory. *IEEE Trans. Power Syst.* **2010**, *25*, 392–403. [[CrossRef](#)]
21. Duong, M.Q.; Grimaccia, F.; Leva, S.; Mussetta, M.; Le, K.H. Improving transient stability in a grid-connected squirrel-cage induction generator wind turbine system using a fuzzy logic controller. *Energies* **2015**, *8*, 6328–6349. [[CrossRef](#)]
22. Duong, M.Q.; Sava, G.N.; Grimaccia, F.; Leva, S.; Mussetta, M.; Costinas, S.; Golovanov, N. Improved LVRT based on coordination control of active crowbar and reactive power for doubly fed induction generators. In Proceedings of the 2015 9th International Symposium on Advanced Topics in Electrical Engineering (ATEE), Bucharest, Romania, 7–9 May 2015.
23. Takada, H.; Kato, Y.; Iwamoto, S. Transient stability preventive control using CCT and generation margin. In Proceedings of the Power Engineering Society Summer Meeting, Vancouver, BC, Canada, 15–19 July 2001.
24. Kato, Y.; Iwamoto, S. Transient stability preventive control for stable operating condition with desired CCT. *IEEE Trans. Power Syst.* **2002**, *17*, 1154–1161. [[CrossRef](#)]
25. Fujii, W.; Wakisaka, J.; Iwamoto, S. Transient stability analysis based on dynamic single machine equivalent. In Proceedings of the 39th North American Power Symposium, Las Cruces, NM, USA, 30 September–2 October 2007.
26. Bae, K.; Thorp, J.S. A stochastic study of hidden failures in power system protection. *Decis. Support Syst.* **1999**, *24*, 259–268. [[CrossRef](#)]
27. Chen, J.; Thorp, J.S.; Dobson, I. Cascading dynamics and mitigation assessment in power system disturbances via a hidden failure model. *Int. J. Electr. Power Energy Syst.* **2005**, *27*, 318–326. [[CrossRef](#)]
28. Yang, F.; Meliopoulos, A.S.; Kokkinides, G.J.; Dam, Q.B. Effects of protection system hidden failures on bulk power system reliability. In Proceedings of the 38th North American Power Symposium, 2006 (NAPS 2006), Carbondale, IL, USA, 17–19 September 2006.
29. Salim, N.A.; Othman, M.M.; Musirin, I.; Serwan, M.S. Determination of sensitive transmission lines due to the effect of protection system hidden failure in a critical system cascading collapse. *Int. J. Electr. Comput. Energ. Electron. Commun. Eng.* **2013**, *7*, 548–553.
30. Chen, G.; Dong, Z.Y.; Hill, D.J.; Zhang, G.H.; Hua, K.Q. Attack structural vulnerability of power grids: A hybrid approach based on complex networks. *Phys. A Stat. Mech. Appl.* **2010**, *389*, 595–603. [[CrossRef](#)]
31. Probability Methods Subcommittee. IEEE reliability test system. *IEEE Trans. Power Appar. Syst.* **1979**, *PAS-98*, 2047–2054.
32. Grigg, C.; Wong, P.; Albrecht, P.; Allan, R.; Bhavaraju, M.; Billinton, R.; Chen, Q.; Fong, C.; Haddad, S.; Kuruganty, S.; et al. The IEEE reliability test system-1996. A report prepared by the Reliability Test System Task Force of the Application of Probability Methods Subcommittee. *IEEE Trans. Power Syst.* **1999**, *14*, 1010–1020.
33. Dobson, I.; Newman, D.E. Cascading blackout overall structure and some implications for sampling and mitigation. *Int. J. Electr. Power Energy Syst.* **2017**, *86*, 29–32. [[CrossRef](#)]

